Supporting Information for

Novel Statistical Analysis Illustrates Importance of Flow Source for Extreme Variation in Dissolved Organic Carbon in a Eutrophic Reservoir in the Great Plains

Anthony A. P. Baron[1], Helen M. Baulch[1,2], Ali Nazemi[3], Colin J. Whitfield[1,2]

[1]School of Environment and Sustainability, University of Saskatchewan, Saskatoon, S7N 5C5, Canada.
[2]Global Institute for Water Security, University of Saskatchewan, Saskatoon, S7N 3H5, Canada.
[3]Department of Building, Civil and Environmental Engineering, Concordia University, Montréal, H3H 2L9, Canada.

Correspondence to: Anthony A. P. Baron (anthony.baron@usask.ca)

S1 Introduction

In this supplementary information section we include several tables and figures to support the main text. Table S1 provides the locations, station numbers, and complete flow record details for the four gauging stations used in our analyses, and the estimated period for the ungauged portion of the Buffalo Pound Lake catchment. Table S2 describes the analytical methods used at the Buffalo Pound Water Treatment Plant (BPWTP) ISO/IEC 17025 accredited laboratory, and the sampling frequency and duration for each analyte. In Table S3 summary statistics for all streamflow and water chemistry parameters are presented. Figure S1 shows the wavelet transform of each environmental predictor. Figure S2 depicts the average wavelet coherence between dissolved organic carbon (DOC) and each environmental predictor, along with coherence bands at short (< 18-month) and long (> 18-month) timescales for all parameters. Figure S3 displays the wavelet phase relationships for the same parameters at short and long timescales. Figure S4 shows four model diagnostics of the GAM fitted to DOC concentration presented in the main text (Figs. 5 and 6). Figure S5 and S6 show long-term patterns of DOC:DON (DOC:dissolved organic nitrogen) and SUVA (specific ultraviolet absorbance at 254 nm normalized to DOC concentration) respectively.

Table S1. Site names, abbreviations, Water Security Agency gauging station numbers, geographic coordinates, and gauged and estimated flow records for five contributing streams and areas above Buffalo Pound Lake.

Site name	Symbol	Station number	Coordinates	Flow record
Lake Diefenbaker outflow	Q_{LD}	SK05JG006	50.97ºN, 106.39ºW	Gauged 1972–2019
Ridge Creek	Q_{RC}	SK05JG013	50.95ºN, 106.32ºW	Gauged 1972–2019
Iskwao Creek	Q_{IC}	SK05JG014	50.97ºN, 105.95ºW	Gauged 1972–2006 (warm season); estimated 1990–2006 (cold season) and 2007–2019
Buffalo Pound Lake inflow	Q_{BP}	SK05JG004	50.78ºN, 105.82ºW	Complete records 1968–1994 and 2016–2019; estimated 1995–2015
Ungauged	Q_{U}	—	—	Estimated 1993–2019

Table S2. Analytical methods (APHA, 2012) used at the BPWTP ISO/IEC 17025 accredited laboratory, and sampling frequency and duration. Analytical instruments reported here correspond to current methods used by the BPWTP. All instrument changes between 1990 and 2019 were cross validated and subjected to testing requirements associated with accreditation (B. Kardash pers. comm.). MM refers to the plant's Methods Manual procedures, with these methods based on APHA (2012) methods.

Analyte	Unit	Laboratory method or APHA method	Method summary (current instrumentation noted)	Sampling frequency
DOC	mg C L^{-1}	MM #20, v. 2.1; APHA Method 5310A and C	1990–2014: organic carbon oxidized to CO_2 is measured using a Tekmar/Dohrmann Phoenix 8000 Carbon Analyzer; 2015–2019: total (dissolved) organic carbon and DIC are separated into conductivity cells by gas-permeable membrane to separate CO_2, then measured conductivity in each cell is used to calculate DOC and DIC	Weekly (1990–2019)
SO_4^{2-}	mg S L^{-1}	MM #3, v.2.7; modified from APHA Method 4110B	Ion chromatography using a Dionex ICS-1100 Ion Chromatograph	Weekly (1990–2002); semi-monthly to monthly (2003–2019)
TP[(a)]	µg P L^{-1}	MM #202, v. 3.1; APHA Methods 4500-P B(5) and D	Digestion with strong acid and persulfate [APHA Method 4500-P B(5)] followed by colorimetric analysis using molybdenum blue method at 690 nm [APHA Method 4500-P D]	Weekly (1990–2002); semi-monthly to monthly (2003–2019)
SRP[(a)]	µg P L^{-1}	MM #203, v. 3.1; APHA Method 4500-P C	Soluble phosphorus ions complexed with ammonium molybdate to form ammonium-phosphomolybdate and reduced to molybdenum blue with stannous chloride, then absorbance measured at 690 nm	Weekly (1990–2002); monthly (2003–2019)
Chl α[(a)]	µg L^{-1}	MM #206, v. 2.1; APHA Method 10,200-H 1&2	Extraction of filtrate using aqueous acetone, and analysis via spectrophotometer as per APHA Method 10,200-H with the modification that results are not corrected for pheophytin α or pheophorbide α.	Weekly (1990–2002); monthly (2003–2012); weekly to semi-monthly (2012–2019)
NO_3^-–N[(a)]	mg N L^{-1}	MM #3, v. 2.3; APHA Method 4110-A, B, C	Ion chromatography using a Dionex ICS-1100 Ion Chromatograph	Weekly (1990–2002); semi-monthly to monthly (2003–2019)
NH_4^+–N[(a)]	mg N L^{-1}	MM #201, v. 2.2 APHA Method 4500-P C	Water sample is buffered at pH 9.5 with a borate buffer and distilled into a boric acid solution. Ammonia in the distillate is then determined colorimetrically by addition of Nessler's reagent	Weekly (1990–2002); semi-monthly to monthly (2003–2019)

(a) Method summary from Cavaliere and Baulch (2020)

Table S3. Summary statistics for DOC concentration and eight environmental predictors (1990–2019). The real number of observed values *N* is reported here; where *N* < 360 missing values were imputed using *k* = 1 nearest neighbour regression (Altman, 1992; Fix and Hodges, 1951). Abbreviations: Q1 – first quartile; Q3 – third quartile; LOQ – limit of quantification.

Parameter	Unit	*N*	Minimum	Median	Q1	Q3	Maximum
DOC	mg C L^{-1}	360	3.3	6.3	5.5	7.9	12.4
SO_4^{2-}	mg S L^{-1}	359	56.8	117.4	95.7	156.4	339.8
TP	µg P L^{-1}	351	14	63	48	85	232
SRP	µg P L^{-1}	350	< LOQ	10	6	18	99
Chl *a*	µg L^{-1}	355	< LOQ	16	9	27	151
NO_3^-	mg N L^{-1}	358	< LOQ	0.04	0	0.11	1.54
NH_4^+	mg N L^{-1}	348	< LOQ	0.08	0.03	0.13	0.45
Q_{LD}	m^3 s^{-1}	360	0	2.2	1.5	4.1	12.4
Q_{BP}	m^3 s^{-1}	360	0.1	2.6	1.6	4.7	18.9
Q_{LC}	m^3 s^{-1}	360	0	0	0	0.2	8.3

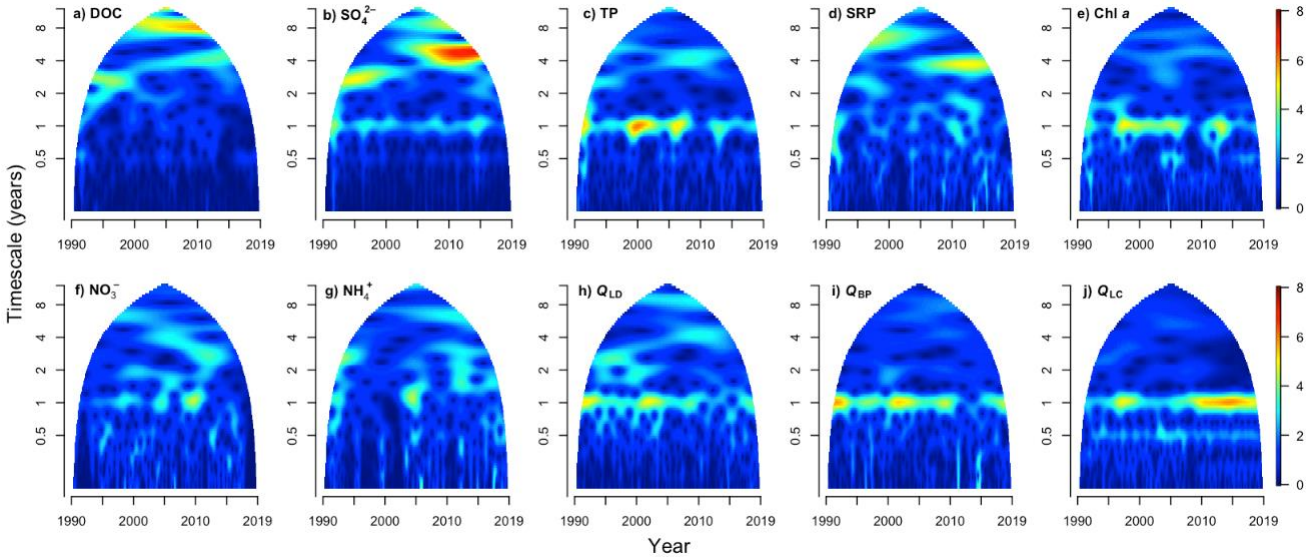

Figure S1. (a–j) Wavelet transforms of DOC, TP, SRP, SO_4^{2-}, Chl *a*, NO_3^-, NH_4^+, Q_{LD}, Q_{LC}, and Q_{BP} showing the magnitude of the transform (*z*-axis, colour bar) against time (*x*-axis) and timescale (*y*-axis). Note the *y*-axis is log-transformed. The wavelet transform is based on a convolution of a wavelet function with the time series (Reuman et al., 2021). Because of this, times and timescales where the overlap of the wavelet transform with the time series is insufficient and unreliable are omitted. The 'rocket ship nose cone' plot results from omission of these regions (i.e., at times closer to the edges of the time series). At long timescales more values are omitted because long-timescale wavelets extend over the end of the time series further in the convolution computation.

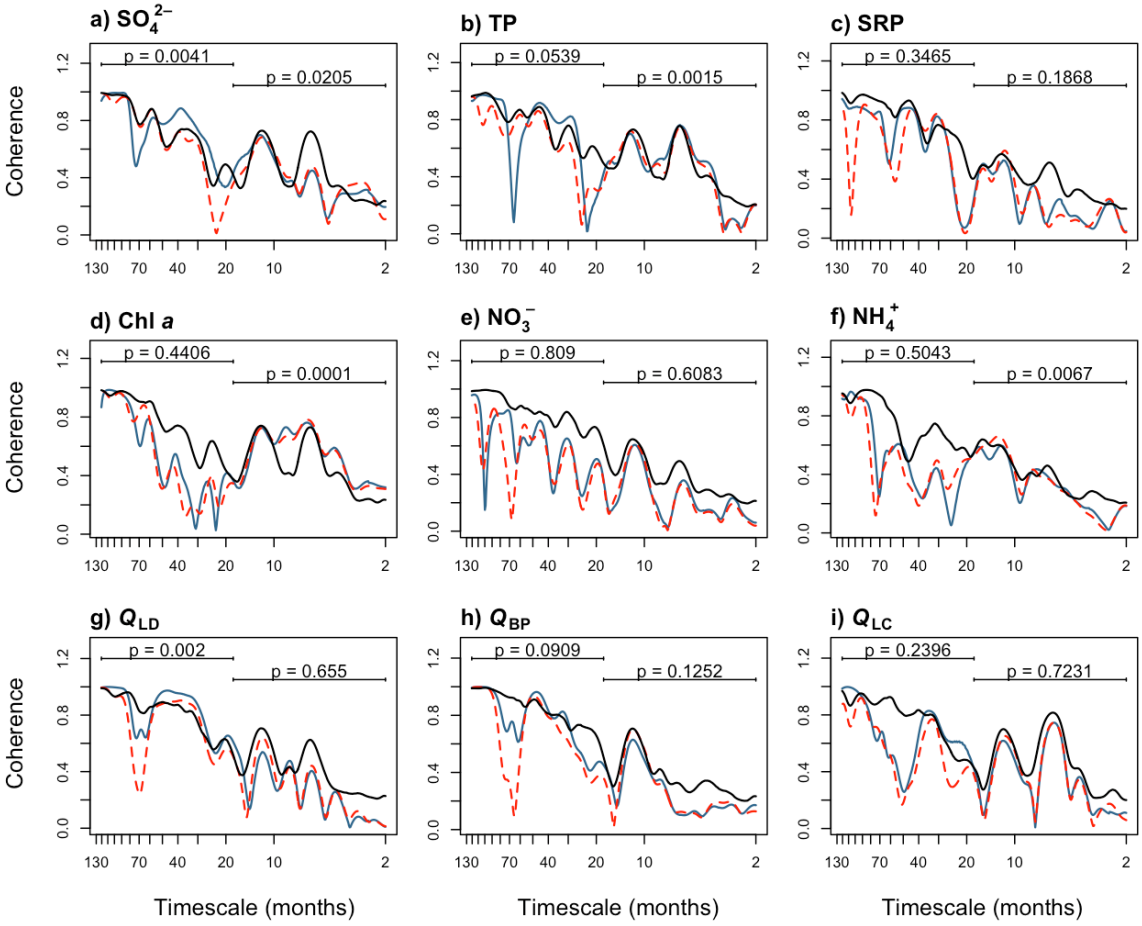

Figure S2. (a–i) Wavelet coherence using the wavelet mean field (Sheppard et al., 2016) for nine DOC–environmental predictor pairs. Coherence magnitude (*y*-axis, range 0–1) represents the sum of the mean squared magnitude of the wavelet mean field over all timescales. The *x*-axis (log scale, reversed) depicts the range of timescales (2 to 120 months) for which coherence can be reliably investigated for each time series (1/3 of the total length of the original time series). The blue solid line is coherence. The solid black line is the 95th quantile of coherences of surrogate data sets (n = 10,000 surrogates). Coherence is significant ($\alpha < 0.05$) for timescales in which the red dashed line is above the black line. Bars above the coherence line are timescales over which coherence was tested for significance. Timescales are defined as short (≤ 18 months) and long (> 18 months).

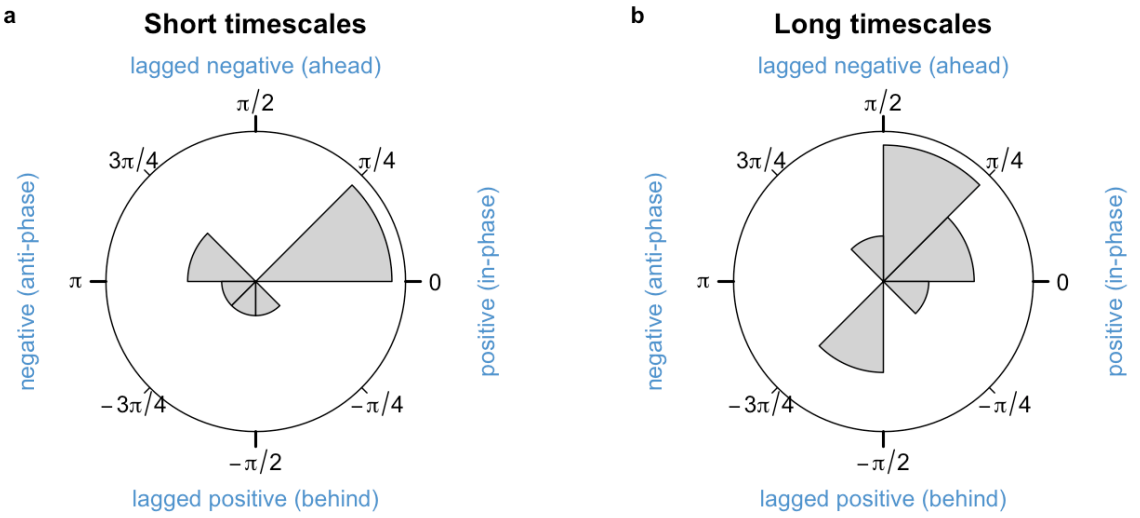

Figure S3. Distributions of phase differences at (a) short (≤ 18-month) and (b) long (> 18-month) timescales for all environmental predictors and DOC concentration. Radius length is proportional to the frequency of each type of relationship observed (lagged, in-phase, anti-phase), where longer radii indicate higher frequency (as in (a)). Lagged negative refers to peaks in DOC leading ahead of peaks in a predictor; lagged positive refers to peaks in DOC lagging behind peaks in a predictor. In-phase relationships are analogous to positive correlation, whereas anti-phase relationships are analogous to negative correlation. See Table 1 for details.

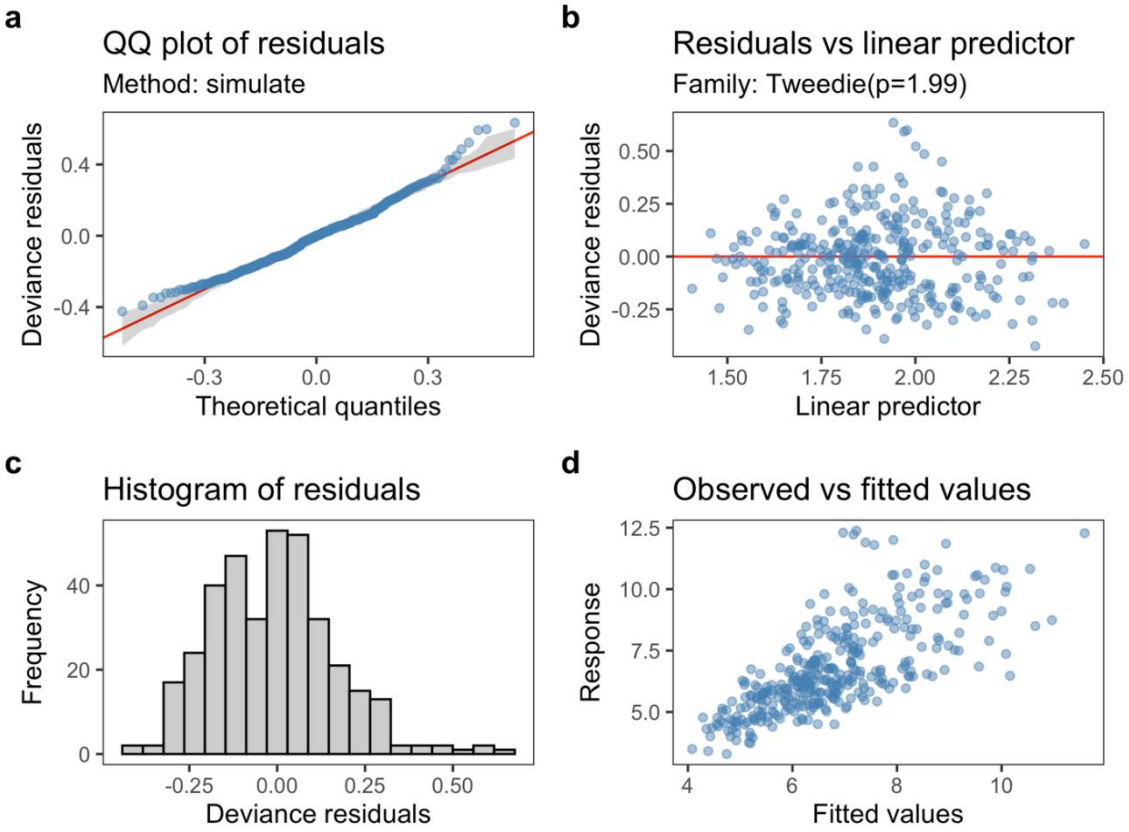

Figure S4. Model diagnostics of the GAM of DOC concentration with SO_4^{2-}, TP, Chl *a*, NH_4^+, and Q_{LD} (Fig. 6 in main text). (a) QQ plot of residuals showing some deviation from normality, which is likely affected by the few extreme high and low DOC concentrations in the 30-year record. (b) Residuals vs linear predictor plot. While there is not a strong pattern in this plot (evidence of relatively good fit), there are several points at the tails of 'Linear predictor' and the higher end of 'Deviance residuals' that suggest relatively high and low DOC concentrations were poorly estimated by this model. (c) Histogram of residuals. Residuals are approximately normally distributed with a few extreme values at the tails. (d). Observed vs fitted values showing the fit between measured (*y*-axis) and modeled (*x*-axis) DOC concentrations. At DOC concentrations < ~8 mg L^{-1} the GAM provides a good fit to the data; however, at concentrations > ~8 mg L^{-1} there is often considerable variation between observed and estimated DOC concentrations. At these higher concentrations the coherent environmental predictor covariates struggled to explain variation in DOC.

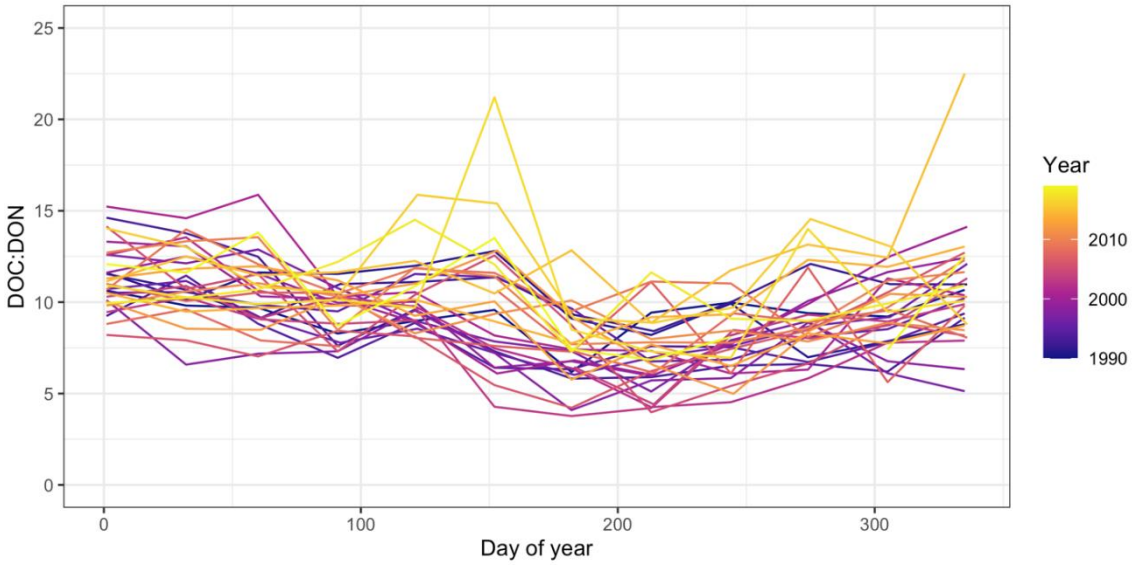

Figure S5. Intraannual variation in DOC:DON at Buffalo Pound Lake between 1990 and 2019.

70

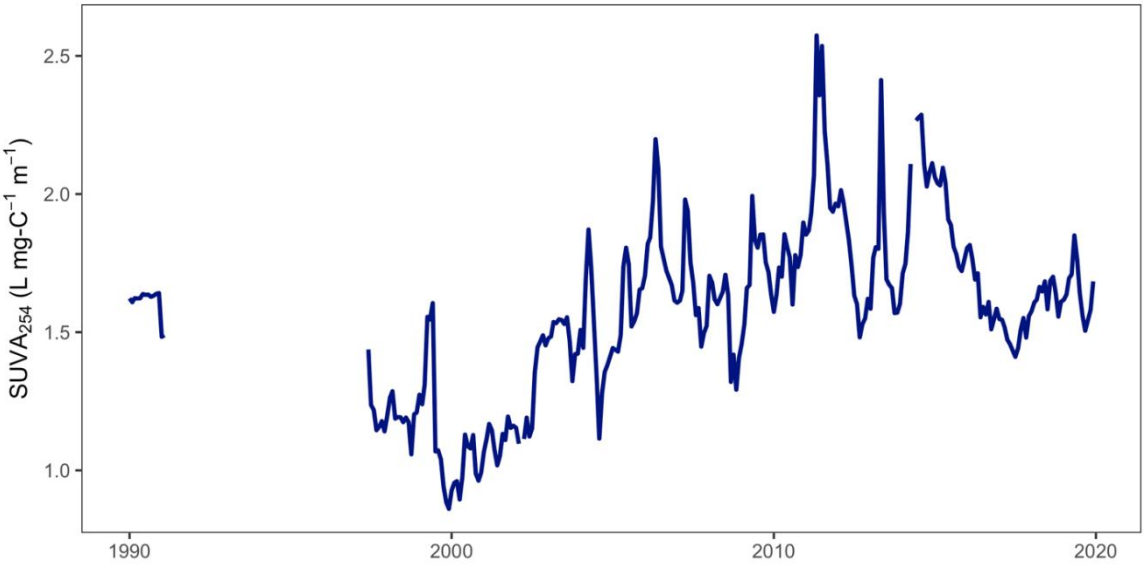

Figure S6. Buffalo Pound Lake ultraviolet absorbance at 254 nm (A_{254}) normalized to DOC concentration (SUVA) from 1990 to early 1991 and late 1997 to 2019, calculated as A_{254} divided by DOC concentration.

References

Cavaliere, E., Baulch, H.M., 2020. Winter in two phases: Long-term study of a shallow reservoir in winter. Limnol. Oceanogr. 9999, 1–18. https://doi.org/10.1002/lno.11687

Sheppard, L.W., Bell, J.R., Harrington, R., Reuman, D.C., 2016. Changes in large-scale climate alter spatial synchrony of aphid pests. Nat. Clim. Chang. 6, 610–613. https://doi.org/10.1038/nclimate2881